Investigation of $C_{60}F_{36}$ as low-volatility *p*-dopant in organic optoelectronic devices

Rico Meerheim,[1,a)] Selina Olthof,[1] Martin Hermenau,[1] Sebastian Scholz,[1] Annette Petrich,[1] Nir Tessler,[2] Olga Solomeshch,[2] Björn Lüssem,[1] Moritz Riede,[1] and Karl Leo[1,b)]
[1]*Institut für Angewandte Photophysik, Technische Universität Dresden, George-Bähr-Straße 1, 01062 Dresden, Germany*
[2]*Electrical Engineering Department, Nanoelectronic Center, Technion, Haifa 32000, Israel*

(Received 3 October 2010; accepted 9 April 2011; published online 16 May 2011)

We demonstrate highly efficient small molecule organic light emitting diodes and organic solar cells based on the *p-i-n*-type structure using the fluorinated fullerene molecule $C_{60}F_{36}$ as *p*-dopant in the hole transport layer. We present synthesis, chemical analysis, and energy level investigation of the dopant as well as the conductivity of organic layers consisting of a matrix of N,N,N′,N′-tetrakis 4-methoxyphenyl-benzidine(MeO-TPD) or N,N′-[(Diphenyl-N,N′-bis)9, 9,-dimethyl-fluoren-2-yl]-benzidine(BF-DPB) doped by the fullerene compound. State of the art organic *p-i-n* devices containing $C_{60}F_{36}$ show efficiencies comparable to devices with the commonly used *p*-dopant2,3,5,6-tetrafluoro-7,7,8,8-tetracyanoquinodimethane (F_4-TCNQ). The advantages of the fullerene based dopant are the low volatility and high thermal stability, which is beneficial for device operation under elevated temperature. These properties make $C_{60}F_{36}$ highly attractive for the usage as *p*-dopant in a broad spectrum of organic *p-i-n* devices like organic light emitting diodes, solar cells, memories, or transistors. © *2011 American Institute of Physics*. [doi:10.1063/1.3590142]

I. INTRODUCTION

In recent years, the performance of organic devices such as organic light emitting diodes (OLED) and solar cells (OSC) has been improved significantly by employing the concept of *p* and *n* doping of the charge transport layers.[1,2] In this concept, it is desirable to use molecules as dopants since they are less prone to diffuse in a matrix layer compared to doping by alkali metals or other low weight compounds. Some *p*-doping example molecules with a high electron affinity (EA) are the weak donor tetracynoquinodimethane (TCNQ)[3,4] or the fluorinated versions 3,6-difluoro-2,5,7,7,8,8-hexacyanoquinodimethane(F_2-HCNQ)[5] and the currently most common2,3,5,6-tetrafluoro-7,7,8,8-tetracyanoquinodimethane (F_4-TCNQ).[6,7] By introducing a low molar ratio of such an electron acceptor in a host material, e.g., N,N,N′,N′-tetrakis 4-methoxyphenyl-benzidine (MeO-TPD), a charge transfer can take place as long as the EA of the dopant is larger than the ionization potential (IP) of the host. Using the concept of electrical doping, the conductivity of the transport layers can be increased by several orders of magnitude[8] which substantially increases the device efficiency by reducing the operating voltage in OLEDs and lowering the series resistance in OSC. Furthermore, the charge injection barrier at the contacts is reduced due to the shift of the Fermi energy in the hole transport layer toward the charge carrier level and the formation of a thin (a few nm) depletion region that can easily be tunneled through by the charge carriers.[9] Hence, the currently most efficient monochrome[10] and white[11] OLEDs, as well as organic solar cells[12] are using molecularly doped layers.

The most commonly used *p*-dopant F_4-TCNQ has the disadvantage of a rather high volatility which can causes problems during the evaporation process leading to a contamination of subsequent organic layers.[13] In emission layers e.g., dopant residuals can act as quenching centers for excitons which reduce the device efficiency. Furthermore, the conductivity of F_4-TCNQdoped layers is not stable at elevated temperatures which can reduce the device lifetime.[14]

In this paper, we compare the *p*-dopants F_4-TCNQ and the fluoro-fullerene $C_{60}F_{36}$ that has recently been reported to act as a solvable *p*-dopant in polymer layers.[15] The fluorination of the C_{60} molecule leads to a lowering of the energy level of around 1 eV,[16] hence an efficient charge transfer from the HOMO of a matrix material with an IP close to 5 eV to the $C_{60}F_{36}$ LUMO, i.e., a doping effect, can occur. Both dopants are investigated regarding their stability, volatility, and application in OLEDs and OSCs. We are able to show that both dopants lead to excellent device performance, with the $C_{60}F_{36}$ molecule having superior processing properties.

A. Dopant synthesis and analysis

The $C_{60}F_{36}$ is synthesized using a method similar to the one published by Boltalina *et al.*[17] Prior to the synthesis, the materials C_{60} (Moskau, KurtchatovInstitut, three times sublimated) and MnF_3 (ABCR, purity 98%) are dried in a high vacuum chamber ($p \sim 10^{-3}$mbar) at 200 °C for 24 h to remove residual water and oxygen contamination. Afterwards, the two materials are mixed (600 mg C_{60} and a typical molar excess of 2.88 g MnF_3) and fine ground under

a)Electronic mail: rico.meerheim@iapp.de.
b)Electronic mail: karl.leo@iapp.de.

nitrogen atmosphere. Boltalina *et al.*[17] used a Ni tube to promote the reaction; however no significant throughput was found using such a setup. Therefore, 10 wt. % of Ni powder are added to the mixed reactants and is found to be a crucial catalyst, and additionally the mixture is placed in a Ni crucible mounted in a regular sublimation tube.[18] The reaction takes place at a pressure of 4×10^{-4} mbar and a crucible temperature of 330 °C in the course of 24 h. The reaction products condense at the colder parts of the tubes where regions of different colors can be found, ranging from brown to yellow and to white with decreasing wall temperature [Fig. 1(a)]. For later use, only the yellow and orange parts of the material are collected as indicated in Fig. 1(a), which corresponds to a yield of 42 wt. %. Due to the application of three novel approaches, (i) the use of Ni powder as a catalyst, (ii) the combination of a the reaction vessel and a sublimation tube within one reaction tool and (iii) the use of a high vacuum within the sublimation tube, the synthesis shows high yields, comparable or even larger than other publications.[17] To ensure a very high purity required for the application of the material in optoelectronic devices, the $C_{60}F_{36}$ is purified once more in the sublimation tube under the same conditions as before. An image of the sublimation tube after this step is shown in Fig. 1(b) and only the indicated rings are used for characterization and device fabrication. The yield of the fullerene dopant after this second purification step is 38.1 wt. %. All further organic materials used in the layers and devices are commercially available and are sublimated at least once to avoid trap states for charge carriers and excitons.[18]

In Fig. 1(c) the spectra of the electron impact ionization mass spectrometry (EI-MS) of the sublimated fluoro-fullerene powder is presented. The spectrum is taken at 70 eV ionization energy and shows the purity of the material. No contribution of the educt C_{60} at 720 amu (atomic mass unit) is visible. The dominant main peak at 1404 amu presents the product $C_{60}F_{36}$ in the first charged state. No higher fluorinated species are detected. Only a minor contribution of an oxidized $C_{60}F_{36}$ compound ($C_{60}F_{36}O_1$) at 1420 amu is visible. Furthermore, the lower fluorinated species $C_{60}F_{34}$ at 1366 amu and the possible EI-MS fragment $C_{60}F_{35}$ of $C_{60}F_{36}$ at 1385 amu can be seen as minor side products. The signal at 702 amu indicates the two times charged $C_{60}F_{36}$, which is a normal artifact in EI-MS measurements.

In the inset of Fig. 1(c) the corresponding Fourier transform infrared absorption (FT-IR) measurement in attenuated total reflection geometry (ATR) of the dopant is visible. Similar to the findings of Boltalina *et al.*,[17] the contribution of the carbon double bonds at wave numbers around $n = 1600$ cm^{-1} is suppressed due to the high fluorination of the material and due to the low content of other reaction products like C_{60} or less fluorinated compounds. Only the very pronounced signal of $C_{60}F_{36}$ at 1030 cm^{-1} is visible which once more indicates the high purity of the synthesized dopant material.

B. Dopant properties

First, we determine the electron affinity of the synthesized dopant to estimate its doping strength. From photoluminescence measurements on a 40 nm thick $C_{60}F_{36}$ layer, an optical HOMO-LUMO gap of 2.5 ± 0.1 eV is obtained. From a recent paper by Djurovich *et al.* that correlates optical gaps with transport gaps via the exciton binding energies by an empirically found relation,[19] we can estimate a transport gap of approximately 3.0 ± 0.3 eV. Considering the ionization potential of 8.38 eV measured by ultraviolet photoelectron spectroscopy (UPS), an electron affinity of 5.38 ± 0.3 eV can be approximated; this is comparable to the electron affinity of F_4-TCNQ which is EA = 5.24 eV.[6] Such a high dopant electron affinity is the prerequisite for an efficient host-guest charge transfer, i.e., doping of hole transport materials like MeO-TPD with an ionization potential of 5.1 eV that was determined by UPS. The found EA and IP values of $C_{60}F_{36}$ do not coincide with previously reported values of IP = 7.3 eV and EA = 4.4 eV.[15] However, these values were measured by cyclovoltammetry which determines the molecule properties in solution and can therefore differ from values measured in a bulk material.

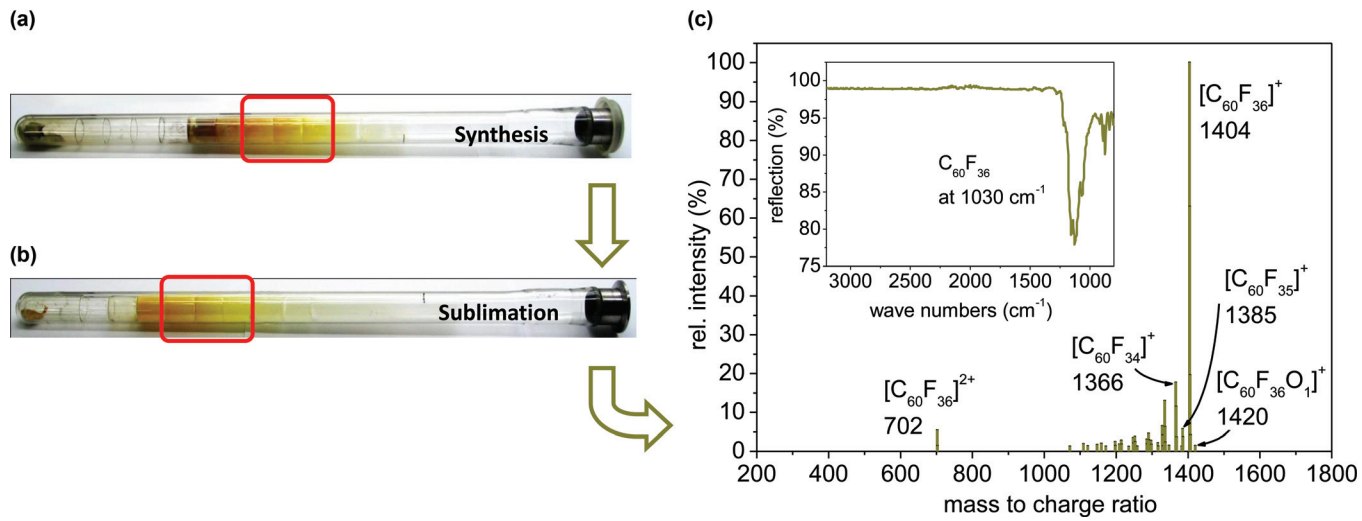

FIG. 1. (Color online) Pictures of the synthesis and sublimation of the *p*-dopant $C_{60}F_{36}$ as well as analysis results. (a) Synthesis and (b) purification of $C_{60}F_{36}$ by vacuum temperature gradient sublimation. For further use only the marked regions of the sublimation tubes are used. (c) Mass spectrum and infrared absorption spectrum of the purified fullerene dopant that show a pronounced signal of the dopant material $C_{60}F_{36}$.

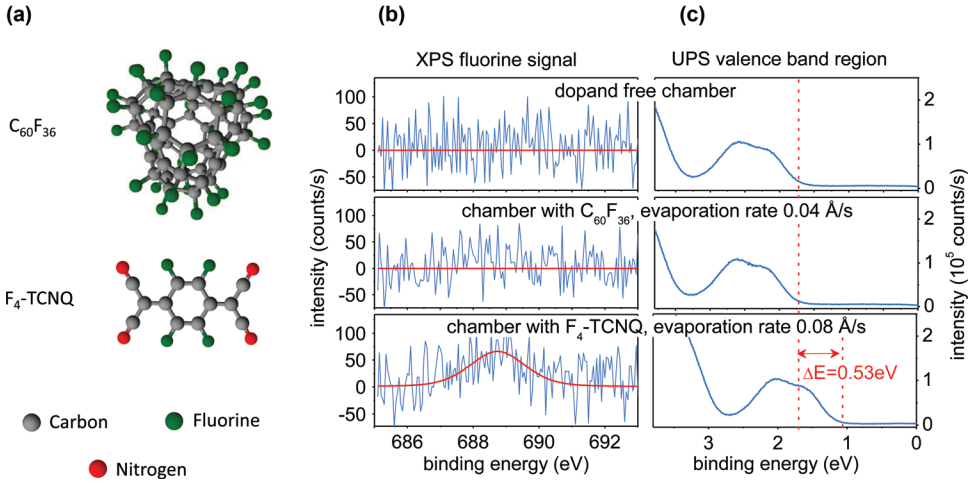

FIG. 2. (Color online) Measurement of the volatility of the *p*-dopants F_4-TCNQ and $C_{60}F_{36}$. (a) Molecular structures of both dopants. (b) XPS and (c) UPS spectra of intentionally intrinsic MeO-TPD layers, made in a dopant-free chamber or in a chamber equipped with either $C_{60}F_{36}$ or F_4-TCNQ in unheated crucibles. Only when F_4-TCNQ is present in the chamber the XPS measurements show traces of fluorine in the layer and at the same time the UPS spectra show a strong HOMO level shift of the MeO-TPD layer by 0.53 eV.

In a further experiment, we evaluate the volatile behavior of F_4-TCNQ and $C_{60}F_{36}$ [Fig. 2(a)] by comparing the intensity of the dopant related fluorine signal using x-ray photoelectron spectroscopy (XPS) in intentionally undoped MeO-TPD samples. MeO-TPD is a commonly used standard hole transport material. Figure 2(b) shows a comparison of the fluorine 1s core level signal of the XPS measurement of the 10 nm thick intrinsic MeO-TPD layers that are evaporated at very low rates in a chamber containing either one of the two dopants in an unheated crucible or in a dopant free chamber. The Lorenz−Gauss curve fits show a measurable fluorine signal at 689.5 eV only when the chamber is equipped with F_4-TCNQ which proves contamination by the presence of the volatile F_4-TCNQ molecules. However, when the chamber contains $C_{60}F_{36}$ molecules, no fluorine 1s core signal and thus, no contamination in the MeO-TPD layer is observed. Furthermore, a doping effect by the F_4-TCNQ contamination can be found in UPS experiments [Fig. 2(c)]. The Fermi level position (at $E_B = 0$ V) is identical for the layers evaporated in the dopant free chamber and in the chamber containing $C_{60}F_{36}$, whereas a shift of 0.53 eV toward the HOMO is observed for the layer prepared in the chamber containing F_4-TCNQ, clearly indicating a *p*-doping of the layer. The low volatility of $C_{60}F_{36}$ in comparison with F_4-TCNQ is a significant advantage of the fluoro-fullerene and a strong argument to use this dopant in hole transport layers.

Subsequently, the temperature stability of the doped layers is tested in hole transport layers consisting of N,N′-[(Diphenyl-N,N′-bis)9,9,-dimethyl-fluoren-2-yl]-benzidine (BF-DPB) [Fig. 3(a)] co-evaporated with either F_4-TCNQ or $C_{60}F_{36}$ which is shown in Fig. 3(b). The alternative host material is used due to its exceptionally high glass transition temperature (T_G) of 160 °C (product information from the supplier Sensient Technology Corporation). Thus, it can be assured that a degradation of the dopant and not a change of the layer morphology[20] of the matrix molecules are responsible for the breakdown on conductivity. At molar ratios of 0.26 for F_4-TCNQ and 0.21 for $C_{60}F_{36}$, the 30 nm thick layers show a comparable conductivity of 3×10^{-6} S/cm at room temperature. The fact that a lower molar ratio of the dopant $C_{60}F_{36}$ is needed compared to F_4-TCNQ shows that

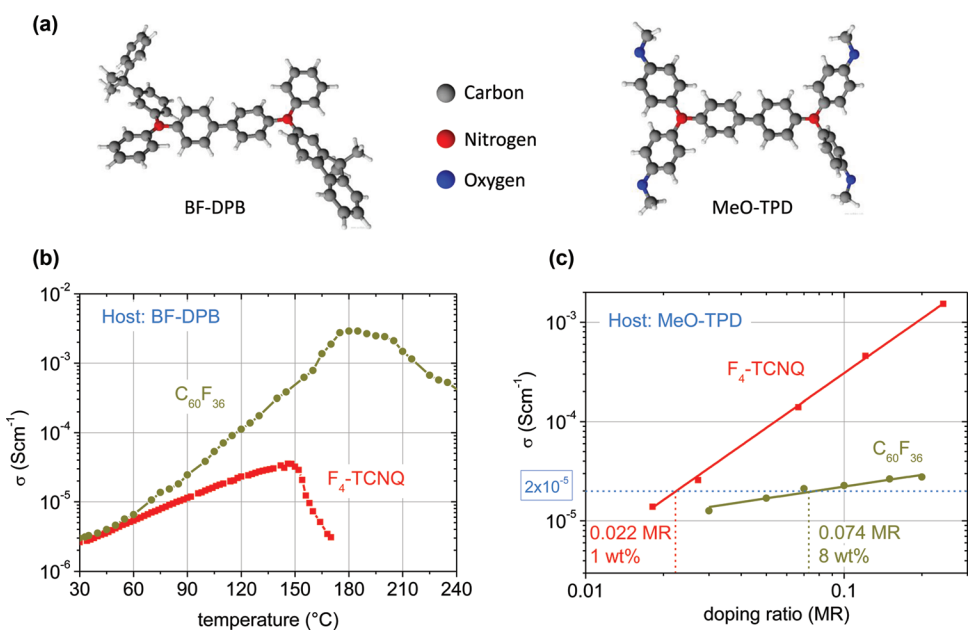

FIG. 3. (Color online) Physical properties of hole transport layers containing the *p*-dopants F_4-TCNQ or $C_{60}F_{36}$. (a) Molecular structures of the used host materials BF-DPB and MeO-TPD. (b) Conductivity of 30 nm thick BF-DPB layers doped by a molar ratio of 0.26 F_4-TCNQ or 0.21 $C_{60}F_{36}$ as a function of substrate temperature. A significantly higher thermal stability of the layer doped by $C_{60}F_{36}$ is found. (c) Conductivity of MeO-TPD layers doped by either F_4-TCNQ or $C_{60}F_{36}$ as a function of molar doping ratio. The $C_{60}F_{36}$ shows a weaker doping effect per molecule and a slower conductivity increase.

$C_{60}F_{36}$ has a higher doping efficiency, i.e., a better charge transfer per molecule within the host BF-DPB. The IP of BF-DPB measured by UPS is 5.23 eV which is comparable to the electron affinity of F_4-TCNQ and leads to a less efficient charge transfer. Therefore, we can conclude that the EA of the dopant $C_{60}F_{36}$ is indeed higher than F_4-TCNQ. With increasing temperature, both transport layers show an increase of the conductivity with activation energies of 265 and 692 meV for F_4-TCNQ and $C_{60}F_{36}$, respectively, until a maximum temperature is reached where the conductivity breaks down. Here, the higher activation energy of $C_{60}F_{36}$ indicates that deep trap states are formed. This can in general be viewed as a disadvantage of the dopant; however, the higher charge transfer for $C_{60}F_{36}$ still leads to an excellent conductivity of the layer. Most importantly, a significantly lower thermal stability of BF-DPB: F_4-TCNQ is observed with a conductivity breakdown at a temperature of 145 °C when the dopant molecules might break under thermal stress or diffuse out of the layer as e.g. Gao *et al*. have shown for zinc phthalocyanine layers doped with F_4-TCNQ.[7,21,22] For the BF-DPB: $C_{60}F_{36}$ layer, the breakdown happens at 180 °C which is already above the T_G of the host material and therefore not necessarily due to a degradation or diffusion of the dopant.

Finally, we investigate the hole transport conductivity of MeO-TPD layers [Fig. 3(a)] at various doping ratios of either F_4-TCNQ or $C_{60}F_{36}$ [Fig. 3(c)]. The measurement with F_4-TCNQ shows the well known super linear increase in the log-log plot[23] while $C_{60}F_{36}$ shows a sublinear increase. Furthermore, a lower doping efficiency at comparable molar ratio is observed for $C_{60}F_{36}$ in contrast to the findings in BF-DPB. In the case of the low ionization energy host material MeO-TPD the dopant F_4-TCNQ seems to be more efficient even though $C_{60}F_{36}$ was shown to be the stronger dopant in BF-DPB. We believe that in the case of MeO-TPD: $C_{60}F_{36}$, the sublinear conductivity increase is caused by the previously mentioned deep trap states and in addition the large size of this dopant could distort the morphology and decreases the mobility. At molar ratios of 0.022 (F_4-TCNQ) and 0.074 ($C_{60}F_{36}$), a conductivity of 2×10^{-5} S cm^{-1} is reached which is sufficient for efficient hole transport layers in optoelectronic devices. These values correspond to weight percentages of 1 and 8 wt. % for F_4-TCNQ and $C_{60}F_{36}$, respectively and are used for the comparison of the performance of the dopants in OLED and OSC devices discussed below.

C. OLED devices

For the OLED device investigations, we follow the *p-i-n* concept, using an orange-red emitting phosphorescent structure[24] for the comparison of the different *p*-dopants as shown in the device stack of Fig. 4(a). The organic layers are sandwiched in between a 90 nm thick indium tin oxide (ITO) anode on glass and a 100 nm thick silver top electrode. As *p*-type hole injection and transport layer (HTL), we use 60 nm thick films of MeO-TPD doped with either 1 wt. % of F_4-TCNQ or 8 wt. % $C_{60}F_{36}$, exhibiting a conductivity of 2×10^{-5} S cm^{-1}. As *n*-type electron injection and transport layer (ETL), we use 65 nm of Cs doped 4,7-diphenyl-1,10-phenanthroline (BPhen) with a conductivity comparable to the *p*-side. 10 nm of 2,2′,7,7′-tetrakis-(N,N-diphenylamino)-9,9′-spirobifluorene(Spiro-TAD) and 10 nm of BPhen are used as electron and hole blocking layer (EBL, HBL), respectively, to confine electrons and holes in the emitting layer (EML). The 20 nm thick red EML consists of N,N′-di(naphthalen-2-yl)-N,N′-diphenyl-benzidine(alpha-NPD), doped with 10 wt. % of the triplet emitter iridium(III)bis (2-methyldibenzo-[f,h]quinoxaline)(acetylacetonate) [Ir(MDQ)$_2$(acac)].

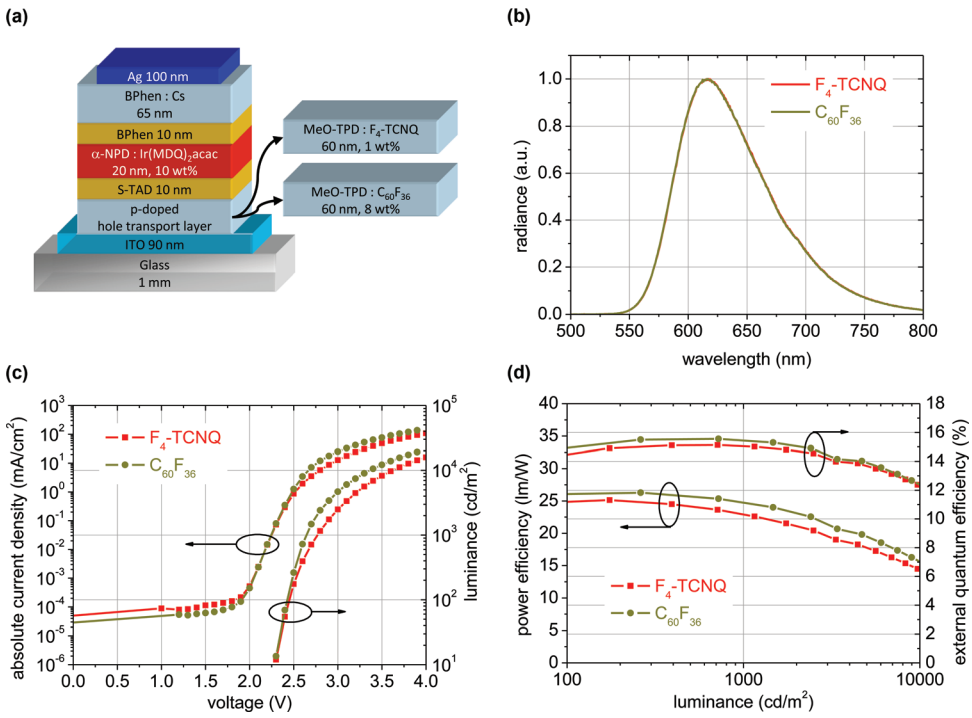

FIG. 4. (Color online) Characteristics of organic light emitting diodes containing F_4-TCNQ or $C_{60}F_{36}$ as *p*-dopant. (a) OLED stack used for the comparison of the dopant performances. (b) Emission spectra of both OLEDs where the identical curves show that there is no additional absorption by $C_{60}F_{36}$. (c) JVL characteristics of *p-i-n* OLEDs where comparable performance is reached for both *p*-dopants, whereas the fluoro-fullerene shows a steeper JVL rise. (d) Power efficiency and external quantum efficiency of the *p-i-n* OLEDs. Comparable characteristics are reached for both *p*-dopants, with slight advantages for the fluoro-fullerene in terms of higher efficiency.

When comparing the *p*-dopants employed in OLED devices, similar results are obtained. The identical electroluminescence spectra in Fig. 4(b) show that $C_{60}F_{36}$ does not cause noticeable additional absorption. The *JVL* curves [Fig. 4(c)] are steeper for devices with the fluorofullerene dopant, indicating a better hole injection since the conductivities of the hole transport layers are the same for the chosen 1 wt. % F_4-TCNQ and 8 wt. % $C_{60}F_{36}$. Accordingly, the slightly higher efficiencies in the device with the fullerene dopant [Fig. 4(d)] should be due to the better charge injection. We can conclude that the replacement of the *p*-dopant F_4-TCNQ by $C_{60}F_{36}$ in *p-i-n* OLEDs leads to a slightly improved device performance with the advantage of the non-volatility of the *p*-dopant during the production process and the higher thermal stability of the doped layer.

D. OSC devices

In order to confirm the functionality of $C_{60}F_{36}$ in organic solar cells, again two devices are produced where the HTL MeO-TPD is either doped by F_4-TCNQ or $C_{60}F_{36}$ [Fig. 5(a)]. Here, the active layer is formed by a 30 nm thick bulk heterojunction of Zinc-Phthalocyanine (ZnPc) and the fullerene C_{60} which are mixed at a volume ratio of 1:1. The subsequent layer of 30 nm C_{60} acts as an additional photovoltaic active layer. Electron transport is achieved by 15 nm of *n*-doped C_{60} with 3 wt. % of Acridine Orange Base (AOB) as *n*-dopant.[25,26] In the first device, F_4-TCNQ is used with 2 wt. % in a 30 nm thick MeO-TPD layer, while in the second device, we use 8 wt. % $C_{60}F_{36}$ in the same host instead. The top contact is formed by 100 nm aluminum.

Only slight differences are distinguishable in the *JV* curves in Fig. 5(b). The short circuit current density J_{SC} under an illumination of 102.5 mW/cm^2 (nearly one sun) is 8.25 mA/cm^2 for the device with F_4-TCNQ as well as for the device with the fluoro-fullerene as dopant. The open-circuit voltage V_{OC} is better for device with F_4-TCNQ. However, with a discrepancy of only 16 mV, the V_{OC} difference is in the range of the measurement error. Taking into account that the fill factor of the device with $C_{60}F_{36}$ is slightly better, the power conversion efficiencies (PCE) are comparable: For the F_4-TCNQ doped solar cell, it is 2.40% while the $C_{60}F_{36}$ doped cell shows a power conversion efficiency of 2.34% for a mismatch-corrected intensity of 102.5 mW/cm^2. The results are summarized in the inset of Fig. 5(b). In terms of device efficiency, the new dopant $C_{60}F_{36}$ is able to replace F_4-TCNQ as well.

II. METHODS

A. Fourier transform infrared spectroscopy (FT-IR)

The FT-IR measurement is performed in the horizontal attenuated total reflection (ATR) geometry with a Thermo Nicolet Avatar 360 E.S.P. The sample is pressed as powder on top of the ATR unit where the reflection between 450 and 4000 cm^{-1} can be collected. The spectrum is summed over three single spectra. A previously collected background signal was subtracted.

B. Electron impact or electron-ionization mass spectrometry (EI-MS)

Mass spectra of $C_{60}F_{36}$ are obtained with a Finnigan MAT 95 mass spectrometer. The material is mounted as powder in a crucible and is gradually heated for several minutes until an end temperature of 360 °C is achieved while every 3 s a spectrum is collected. The evaporated compounds are ionized at 70 eV and the detection occurs for positive ions. The total ion response start at 200 °C and 121 spectra are summarized.

C. Ultraviolet and x-ray photoelectron spectroscopy

UPS and XPS Measurements are performed with a Phoibos100 system (Specs) at room temperature at a base pressure of 1×10^{-10} mbar and the samples are measured without breaking the vacuum. The measurement of the pure dopant layer is performed on an amorphous gold foil (Goodfellow, 99.99% purity) that is cleaned with an argon sputter gun and afterwards covered by 10 nm of $C_{60}F_{36}$. The investigation of the clean and dopant contaminated 10 nm thick MeO-TPD layers are done on Ar cleaned amorphous silver foil (MaTecK, 99l995% purity). For UPS measurements, the He I line (21.22 eV) from a discharge lamp is used with an energy resolution of 130 meV at a pass energy of 3 eV. The spectra are recorded with the sample bias at −8 eV to observe the cutoff of the slowest electrons. For XPS an Al K_α x-ray source (1486.6 eV) with an energy resolution of 400 meV is used at pass energy of 20 eV. The fluorine peak fits are performed with the program XPSPEAK (Version 4.1) using a linear background.

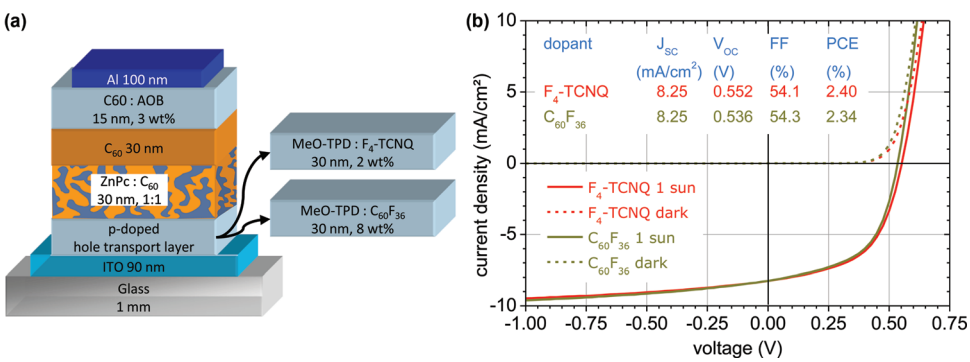

FIG. 5. (Color online) Characteristics of organic solar cells containing F_4-TCNQ or $C_{60}F_{36}$ as *p*-dopant. (a) OSC stack used for the comparison of the dopant performance. (b) *JV* curves of the solar cells with and without illumination with the different dopants in the hole transport layer, measured at 102.5 mW/cm^2. Only slight differences are distinguishable. The inserted table gives the most important device characteristics at an intensity of 102.5 mW/cm^2 (nearly one sun). The power conversion efficiencies are almost identical.

D. OLED and OSC processing and characterization

The OLED and OSC sample preparation is the performed in the same way. All materials are deposited by thermal evaporation from crucibles onto ITO-coated, structured glass substrates in an UHV chamber (Kurt J. Lesker Company) with a base pressure around 10^{-8} mbar. The thickness control during the deposition process is carried out by quartz crystal monitors. The overlap of anode and cathode enclosing the organic layers result in active areas of 6.5 mm^2. The devices are encapsulated immediately after preparation under a nitrogen atmosphere using UV-curing epoxy glue and glass lids. The OLED devices are characterized by an absolute calibrated spectrometer (Instrument Systems CAS 140 CT) by measuring luminance and radiance and a source meter of Keithley (SMU2400) for the *IV* characteristics. The OLED device efficiencies are calculated under the assumption of a Lambertian distribution of radiation. For the illumination of the OSC devices during *IV* measurements, a sun simulator (Optopolymer 16S-150V.3) is used and the intensity is recorded with a certified reference cell. For setting the corrected intensity of 100 mW/cm^2, a spectral mismatch factor of 0.80 is assumed. Afterward, an EQE measurement is carried out to determine the real solar cells spectral mismatch factor to correct intensity as well as J_{SC} and hence the PCE.[27] The self-built setup is composed of a lock-in-amplifier (Signal recovery 4262),a monochromator (Cornerstone 260), and a Xe lamp as light source. Additionally, a filter wheel with a frequency around 90 Hz and a preamplifier (Signal recovery 5182) are used in this setup. The spectrum of the sun simulator, which is also necessary to calculate the mismatch factor, is recorded by a spectrometer (Instrument Systems CAS 140 CT). The real mismatch factor of both observed devices is found to be 0.821. This yields a mismatch corrected intensity of 102.5 mW/cm^2; the values of both J_{SC} and PCE shown are corrected to this value.

ACKNOWLEDGMENTS

The authors thank the BMBF for funding within the projects R2FLEX, InnoProfile, OPA and the State of Saxony for funding within the project NKOE. Furthermore, we want to thank Rene Michel (photoluminescent measurements), Danny Jenner, and Caroline Walde (OLED and OSC sample processing).

[1]K. Walzer, B. Maennig, M. Pfeiffer, and K. Leo, Chem. Rev. **107**, 1233 (2007).
[2]R. Meerheim, B. Lüssem, and K. Leo, Proc. IEEE **97**, 1606 (2009).
[3]M. Maitrot, G. Guillaud, B. Boudjema, J. J. André, and J. Simon, J. Appl. Phys. **60**, 2396 (1986).
[4]R. C. Wheland and J. L. Gillson, J. Am. Chem. Soc. **98**, 3916 (1976).
[5]Z. Q. Gao, B. X. Mi, G. Z. Xu, Y. Q. Wan, M. L. Gong, K. W. Cheah, and C. H. Chen, Chem. Commun. 117–9 (2008).
[6]J. Blochwitz, M. Pfeiffer, T. Fritz, and K. Leo, Appl. Phys. Lett. **73**, 729 (1998).
[7]W.Y. Gao and A. Kahn, Appl. Phys. Lett. **79**, 4040 (2001).
[8]M. Pfeiffer, K. Leo, X. Zhou, J. S. Huang, M. Hofmann, A. Werner, and J. Blochwitz-Nimoth, Org. Electron. **4**, 89 (2003).
[9]J. Blochwitz, T. Fritz, M. Pfeiffer, K. Leo, D. M. Alloway, P. A. Lee, and N. R. Amstrong, Org. Electron. **2**, 97 (2001).
[10]R. Meerheim, R. Nitsche, and K. Leo, Appl. Phys. Lett. **93**, 043310 (2008).
[11]S. Reineke, F. Lindner, G. Schwartz, N. Seidler, K. Walzer, B. Lüssem, and K. Leo, Nature **459**, 234 (2009).
[12]See press release at http://heliatek.de/, April 2010.
[13]B. X. Mi, Z. Q. Gao, K. W. Cheah, and C. H. Chen, Appl. Phys. Lett. **94**, 073507 (2009).
[14]P. Wellmann, M. Hofmann, O. Zeika, A. Werner, J. Birnstock, R. Meerheim, G. He, K. Walzer, M. Pfeiffer, and K. Leo, J. Soc. Inf. Disp. **13**, 393 (2005).
[15]O. Solomeshch, Y. J. Yu, A. A. Goryunkov, L. N. Sidorov, R. F. Tuktarov, D. H. Choi, J.-Il Jin, and N. Tessler, Adv. Mater. **21**, 4456 (2009).
[16]N. Liu, Y. Morio, F. Okino, H. Touhara, O. V. Boltalina, and V. K. Pavlovich, Synth. Met. **86**, 2289 (1997).
[17]O. Boltalina, A. Borschevskii, L. Sidrov, J. Street, and R. Taylor, Chem. Commun. **4**, 529 (1996).
[18]J. Drechsel, A. Petrich, M. Koch, S. Pfützner, R. Meerheim, S. Scholz, K. Walzer, M. Pfeiffer, and K. Leo, SID Dig. Tech. Papers **XXXVII**, 1692 (2006).
[19]P. I. Djurovich, E. I. Mayo, S. R. Forrest, and M. E. Thompson, Org. Electron. **10**, 515 (2009).
[20]K. Walzer, B. Männig, M. Pfeiffer, and K. Leo, Chem. Rev. **107**, 1233 (2007).
[21]J. Birnstock, A. Lux, M. Ammann, P. Wellmann, M. Hofmann, and T. Stübinger, SID Int. Symp. Dig. Tech. Pap. **37**, 1866 (2006).
[22]W. Gao and A. Kahn, Org. Electron. **3**, 53 (2002).
[23]B. Männig, M. Pfeiffer, A. Nollau, X. Zhou, and K. Leo, Phys. Rev. B **64**, 195208 (2001).
[24]R. Meerheim, S. Scholz, S. Olthof, G. Schwartz, S. Reineke, K. Walzer, and K. Leo, J. Appl. Phys. **104**, 014510 (2008).
[25]A. G. Werner, F. Li, K. Harada, M. Pfeiffer, T. Fritz, and K. Leo, Appl. Phys. Lett. **82**, 4495 (2003).
[26]F. Li, M. Pfeiffer, A. Werner, K. Harada, and K. Leo, J. Appl. Phys. **100**, 023716 (2006).
[27]V. Shrotriya, G. Li, Y. Yao, T. Moriarty, K. Emery, and Y. Yang, Adv. Funct. Mater. **16**, 2016 (2006).